

## Exciton Resonances Quench the Photoluminescence of Zigzag Carbon Nanotubes

Stephanie Reich,<sup>1</sup> Christian Thomsen,<sup>2</sup> and John Robertson<sup>1</sup>

<sup>1</sup>Department of Engineering, University of Cambridge, Cambridge CB2 1PZ, United Kingdom

<sup>2</sup>Institut für Festkörperphysik, Technische Universität Berlin, Hardenbergstrasse 36, 10623 Berlin, Germany

(Received 22 December 2004; published 12 August 2005)

We show that the photoluminescence intensity of single-walled carbon nanotubes is much stronger in tubes with large chiral angles—armchair tubes—because exciton resonances make the luminescence of zigzag tubes intrinsically weak. This exciton-exciton resonance depends on the electronic structure of the tubes and is found more often in nanotubes of the +1 family. Armchair tubes do not necessarily grow preferentially with present growth techniques; they just have stronger luminescence. Our analysis allows us to normalize photoluminescence intensities and find the abundance of nanotube chiralities in macroscopic samples.

DOI: 10.1103/PhysRevLett.95.077402

PACS numbers: 78.67.Ch, 71.35.-y, 78.30.Na

A major challenge in research on single-walled carbon nanotubes (SWNTs) is to control and measure the nanotube chiral indices on macroscopic samples. The chiral index  $(n, m)$  fixes the nanotube's diameter and chiral angle. These two parameters determine all properties of a tube, in particular, its electronic structure [1]. Photoluminescence (PL) from SWNTs in solution decreases strongly in intensity for nanotubes with small chiral angles (zigzag tubes) [2–4]. This has been interpreted as reflecting the abundance of  $(n, m)$  nanotubes [2]. If correct, the interpretation has far reaching consequences, because it implies that *most* growth techniques strongly favor armchair over zigzag tubes. Is, however, the luminescence cross section independent of the chiral angle? Can we expect constant maximum luminescence intensities when comparing two tubes of different chirality?

In this Letter, we show that luminescence strongly favors a subset of nanotubes—tubes with a small ratio between their second and first transition energy. This, in particular, implies stronger luminescence for tubes with large chiral angles and from the  $(n - m) \bmod 3 = -1$  family as observed experimentally [2,4]. The chirality dependence arises from an exciton-exciton resonance. This also shifts the experimental optical transition energies to the red compared to the exciton energies. From experimental data, we obtain the exciton energies and maximum luminescence intensities of 40 tube chiralities.

We consider first luminescence in two nanotubes— $(11, 1)$  and  $(10, 2)$ —with similar diameter but very different exciton behavior. Our argument is based on a key observation. The optical transition energies of SWNTs are often shown by the “Kataura plot” in which they vary roughly inversely with tube diameter. The energies deviate systematically above and below this trend [1,5]. This deviation leads to an extra exciton decay channel in tubes with small band gaps.

Figure 1(a) shows the PL process in SWNTs. A photon  $h\nu_{22}$  creates an exciton  $eh_{22}$  in the second subband of the tube, where the index 2 refers to subband 2. The exciton relaxes to the lowest subband  $eh_{11}$  and recombines emitting

the photon  $h\nu_{11}$  [2]. Strong PL occurs if  $h\nu_{22}$  corresponds to a singularity in the excitonic density of states; see Fig. 1(d) [2–4,6]. In the following,  $E_{11}$  ( $E_{22}$ ) denotes the energy of the  $eh_{11}$  ( $eh_{22}$ ) exciton.

Figure 1(a) changes fundamentally if we allow the presence of two excitons in subband 1, which we denote by  $2eh_{11}$  [7]. In a  $(10, 2)$  nanotube,  $E_{22}$  is low so the two-exciton state lies above  $eh_{22}$ . The standard picture is retained [Fig. 1(b)], and the exciton just decays into  $eh_{11}$ . On the other hand, in the  $(11, 1)$  tube,  $eh_{22}$  is high in energy and  $2eh_{11}$  lies below it. When  $eh_{22}$  decays into  $eh_{11}$  [down-pointing dashed arrow in Fig. 1(c)], it liberates enough energy to create a second exciton  $eh_{11}$  (up-pointing dashed arrow). There are two crucial points about this  $eh_{22} \rightarrow 2eh_{11}$  decay: whether it is allowed energetically depends on the nanotube chirality. Two seemingly similar tubes can show very different exciton dynamics. Second,  $2eh_{11}$  has a singular energy dependence [Fig. 1(d)]. Therefore the higher-order process strongly affects the nanotube optical properties. Note that  $eh_{22} \rightarrow 2eh_{11}$  corresponds to electron-electron scattering in graphite, which is the dominant relaxation process for high-energy carriers in that material [8].

In SWNTs in solution, the PL intensity of the  $(11, 1)$  tubes is 3 times weaker than the PL intensity of the  $(10, 2)$

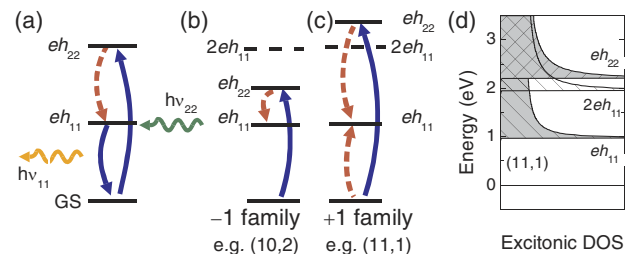


FIG. 1 (color online). (a) PL process:  $eh_{22}$  excitation from the ground state (GS) by photon absorption (solid arrow), relaxation to  $eh_{11}$  (dashed arrow), and emission (solid arrow) of  $h\nu_{11}$ . The relaxation step separates nanotubes into (b) those with only one decay channel and (c) those where  $eh_{22}$  can decay into *two*  $eh_{11}$ ; (d) excitonic density of states (schematic).

tubes [Fig. 2(a)]. This factor was observed in nanotubes grown by different methods [2,4], so it is unlikely to arise from a chirality dependent growth process. The (11, 1) and (10, 2) tubes have very similar diameters (9.0 and 8.7 Å) and chiral angles (4.3° and 8.9°). They are neighbors on the  $(n, m)$  plot of a graphene sheet in Fig. 2(b). The (10, 2) and (11, 1) tubes, however, differ in that they belong to different index families.

SWNTs are characterized by a “family index”  $p = (n - m) \bmod 3$ . Tubes with  $p = 0$  are metallic, and those with  $p = +1$  or  $-1$  are semiconductors [1,5]. For  $+1$  tubes  $E_{22}$  lies above the averaged Kataura trend, while for  $-1$  tubes it lies below this trend [Fig. 3(a)], which comes from trigonal warping and curvature [5,9–11]. This difference carries over into the exciton energies. Tubes with  $p = +1$ , such as (11, 1), have  $E_{22} > 2E_{11}$  as in Fig. 1(c), whereas those with  $p = -1$ , such as (10, 2), have  $E_{22} < 2E_{11}$  as in Fig. 1(b). Now, nanotubes in the

$+1$  family have the extra  $eh_{22} \rightarrow 2eh_{11}$  relaxation channel, which is forbidden in  $-1$  tubes. We argue that this weakens the maximum PL intensity in  $+1$  tubes by broadening their absorption linewidth.

Luminescence depends on the product of the absorption, relaxation, and emission probability. The PL intensity of a tube as a function of excitation energy follows the absorption. The optical matrix elements depend on diameter as  $1/d$ ; their dependences on chiral angle and family cancel due to opposite trends for the second (absorption) and first (emission) subband [12,13]. The PL intensity is hence given by the absorption probability weighted by  $1/d^2$ . Here we assumed constant thermalization rates. For a given tube, this is an excellent approximation [14]. Including the  $(n, m)$  dependence of this step will be an important refinement of our model, but this is beyond the scope of this Letter.

We calculate the absorption spectrum for  $eh_{22}$  by a Green function method [7]:

$$I(E) \propto -\text{Im} \left[ \frac{1}{E - E_{22} + (A\tilde{\alpha}^2 E_{11} / \sqrt{E_{11}^2 - E^2}) + (B^2 \tilde{\alpha}^4 / \sqrt{4E_{11}^2 - E^2})} \right], \quad (1)$$

with a dielectric screening  $\tilde{\alpha} = 0.15$  [7,15], an  $eh_{22} \rightarrow eh_{11}$  coupling  $A\tilde{\alpha}^2 E_{11} \approx 0.01 \text{ eV}^2$ , and an  $eh_{22} \rightarrow 2eh_{11}$  coupling  $B^2 \tilde{\alpha}^4 = 0.1 \text{ eV}^2$ . These parameters fit the electron-hole decay times in SWNTs and graphite [8,16].

Figure 2(a) shows the calculated absorption as a function of excitation wavelength. The (10, 2) absorption shows a single, slightly redshifted Lorentzian [compare arrow at  $E_{22}$  (10, 2)]. In the (11, 1) nanotube, the decay to  $2eh_{11}$  changes the absorption; the strongly redshifted 640 nm peak has a sideband at higher energies (560 nm). By identifying the two narrow peaks in the calculated spectra with the photoluminescence excitation (PLE) maxima (bars), we get excellent agreement in the measured and calculated PLE peak positions and their intensities [Fig. 2(a)]. We find that the maximum PL intensity of a

(11, 1) tube is intrinsically weaker than that of a (10, 2) nanotube [17].

We now generalize our findings to arbitrary SWNT. First we calculate the bare  $eh_{22}$  energies from  $h\nu_{22}$ . We find  $E_{22}$  in a self-consistent routine by requiring the maximum absorption probability in Eq. (1) to occur at  $h\nu_{22}$ . In general,  $h\nu_{22}$  is smaller than  $E_{22}$  because of the redshift

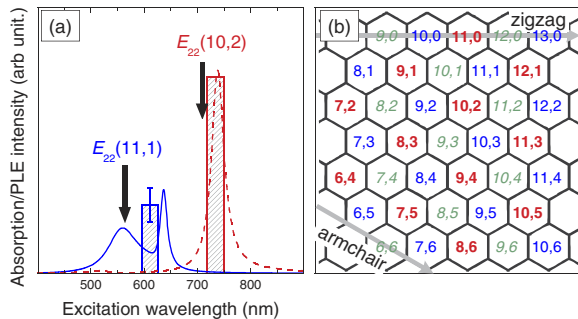


FIG. 2 (color online). (a) Bars: measured wavelength and intensity of the maximum photoluminescence excitation (PLE) signal for the (11, 1) and (10, 2) in solution. The emission is at 0.98 and 1.18 eV for the (11, 1) and (10, 2), respectively [2,4]. Lines: calculated absorption (see text). (b) Tube families:  $p = 0$  (green, italic),  $-1$  (red, bold), and  $+1$  (blue, roman).

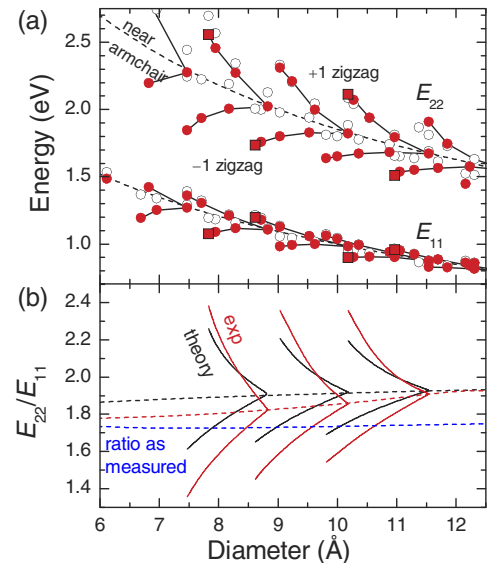


FIG. 3 (color online). (a) Solid symbols: experimental bare exciton energies; open symbols: calculated. Solid lines connect tubes in a branch ( $2n + m = \text{const}$ ); dashed lines tubes with largest chiral angles (close to armchair); squares are zigzag tubes. (b) Ratio of  $E_{22}$  and  $E_{11}$  for three branches. The dashed blue line is the as measured ratio  $h\nu_{22}/h\nu_{11}$  [2].

in Fig. 2(a); see supplement [18].  $E_{11}$  is equal to  $h\nu_{11}$ , since this exciton is not redshifted [2,3]. For comparison we calculated  $E_{ii}$  within the third-order tight-binding approximation [19] using the parametrization by Kane and Mele to account for electron-electron and electron-hole interaction [15].

Figure 3(a) shows the bare exciton energies. Above the isotropic line (black dashed line), the agreement between theory and experiment is excellent; below there are deviations of 10%–20%. These remaining deviations arise from curvature [10,11]. The agreement between theory and experiment systematically improves for large diameters and chiral angles; see Fig. 3(b). For close-to-armchair tubes (dashed lines), experiment matches theory above 11 Å, whereas  $h\nu_{22}/h\nu_{11}$  is constant and 10% smaller than the exciton ratio, which is called the “ratio problem” [2,7].

To calculate a PL map [2] for ensembles of nanotubes, we use  $E_{ii}$  as obtained from  $h\nu_{ii}$  above and find the absorption profile from Eq. (1). We weight the absorption by  $1/d^2$  and the abundance of nanotube chiralities. Here and in the remainder of the Letterer we consider a simulated sample of 78 nanotubes types with a mean diameter of 9.5 Å, a Gaussian diameter distribution of width of 2 Å, typical of HiPCo samples, and *no* preferred chirality.

The calculated PL map in Fig. 4(a) agrees well with the experimental false color plot of Bachilo *et al.* [2] [with the exception of the (11, 0) signature near 750/1040 nm; see discussion of Fig. 4(b)]. For comparison we provide a PL

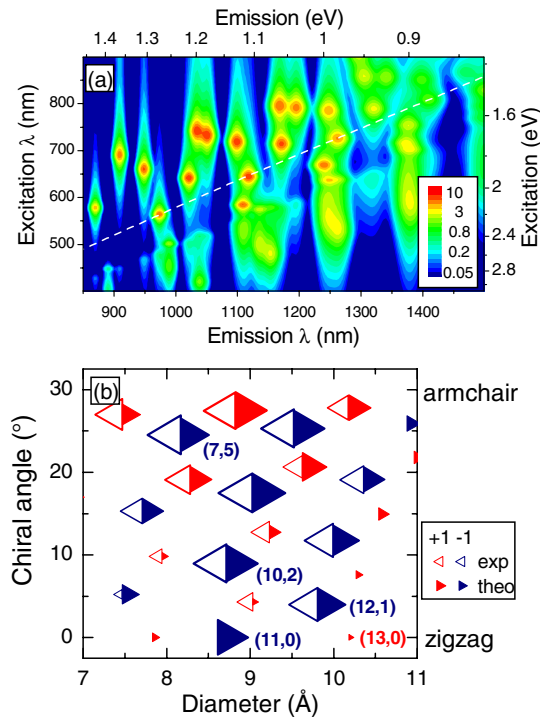


FIG. 4 (color online). (a) Calculated PL for HiPCo nanotubes. The dashed line shows the near-armchair direction. (b) Measured [Fig. 3(d) of Ref. [4]] and calculated PL intensity for HiPCo samples.

map for the same ensemble where we neglected the  $eh_{22} \rightarrow 2eh_{11}$  decay [ $B = 0$  in Eq. (1)] as a supplement [18]. In Fig. 4(a) the intensity is strong for large chiral angles in both semiconducting families. These are the PL peaks close to the armchair direction; see dashed line in Fig. 4(a). Above this line is the  $-1$  family of semiconducting tubes. There are 15 peaks clearly visible in this region. Below the dashed line the plot looks very different in both theory and experiment from above the line. Although there are 14 tubes in this region, we predict only four well defined peaks (compare supplement [18]). They are  $+1$  tubes with large chiral angles. For smaller chiral angles, trigonal warping lowers the  $eh_{11}$  energy, but raises  $eh_{22}$  [5,9]. This effect is enhanced by the curvature of the nanotube wall [10,11]. The  $eh_{22} \rightarrow 2eh_{11}$  resonance sets in; it blurs and broadens the absorption spectra [see Fig. 2(a)]. In the PL map, this creates the vertical streaks.

Figure 4(b) shows the very good agreement between the measured [4] and calculated PL intensities. The intensity of  $-1$  tubes (black or blue) is almost independent of chiral angle; the apparent dependence results from the Gaussian diameter distribution of the tubes [4]. In contrast,  $+1$  tubes (gray or red) show strong luminescence for large angles, but are very weak towards the zigzag direction. PL hardly sees some semiconducting nanotubes at all; e.g., luminescence from a (13, 0) tube (small chiral angle) is 5 times weaker than from a (7, 5) tube. Thus, luminescence is strongly biased towards large chiral angles and nanotubes with  $p = -1$ .

For one tube, the (11, 0), we predicted a strong intensity although it is absent in the measurements [Fig. 4]. This could imply a small abundance of (11, 0) tubes. Alternative explanations, however, are dark excitons below  $eh_{11}$  or electron-phonon interaction [14,20]. The (11, 0) is a singular case in the experimental data as well. The two other  $-1$  tubes with small chiral angles [(10, 2) and (12, 1)] have strong intensities. Two other points are noteworthy: First, our calculations do not predict a constant background for emission above 1000 nm [2]. Further studies are desirable to clarify this experimental background. Second, the absence of features at excitation below 400 and above 850 nm arises from restricting our model to  $eh_{22}$  and  $eh_{11}$  and their interactions.

How can we further verify the model experimentally, and what are the practical implications for finding nanotube abundances? A rigorous test is to compare PL intensities with a chirality distribution from a nonoptical technique, e.g., electron diffraction. This will establish an experimental PL normalization in addition to the theoretical factors given by us [18]. Time-resolved spectroscopy can observe the distinct  $eh_{22} \rightarrow eh_{11}$  and  $eh_{22} \rightarrow 2eh_{11}$  decay channels. The challenge is the weak PL in tubes with the latter decay process. Another prediction from our model is a strong difference between the Raman cross section in resonance with  $eh_{22}$  and  $eh_{11}$ .

The Raman cross section is proportional to the square of the absorption strength. Raman scattering in resonance

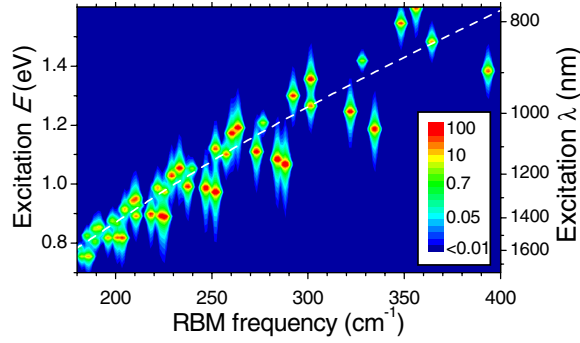


FIG. 5 (color online). Calculated RBM intensity in resonance with  $eh_{11}$  for HiPCo samples [22]. The dashed line shows the near-armchair direction.

with  $eh_{22}$  therefore shows a similar dependence on chirality as PL. It is not exactly the same, because of the squared absorption probability and electron-phonon coupling; see Ref. [21]. For Raman scattering in resonance with  $eh_{11}$ , however, we predict a straightforward way to extract the chirality abundance, because there are no excitonic states below the first subband exciton.

We use the intensities of the radial breathing mode (RBM) reported by Popov *et al.* [22]; although the authors neglected excitons, the dependence of the matrix elements on chirality should be well described by a one-electron model. The Raman intensity map in resonance with  $eh_{11}$  is shown in Fig. 5. In contrast to PL [Fig. 4(a)], Raman scattering shows well resolved peaks for both semiconducting families and all chiral angles.

The maximum Raman intensity in Fig. 5 varies for different RBMs. This comes from the diameter distribution and chirality dependent matrix elements [22]. The latter is described excellently by an analytic function of the diameter  $d$ , chiral angle  $\Theta$ , and family  $p$ . The square root of the Raman intensity follows ( $< 10\%$  deviation)

$$\chi = \left( 1 + p 4.82 \times 10^{-2} + \frac{4.59 \times 10^{-2} d}{\text{nm}} \right) \times [1 + (2.66 \times 10^{-3} + p 6.18 \times 10^{-3}) \Theta + 1.06 \times 10^{-3} \Theta^2] \chi_0, \quad (2)$$

where  $\Theta$  is given in degrees and  $\chi_0$  is constant. Infrared Raman scattering can thus verify our model of exciton decay; it can also be used to normalize the PL dependence on family and chiral angle.

In conclusion, luminescence has a systematically higher cross section for SWNTs with large chiral angles and the  $-1$  family. This arises from a new decay channel when the exciton of the second subband has more than twice the energy of the first subband exciton. The resulting exciton-exciton resonance reduces the maximum absorption strength and shifts the optical transition energies. As an important consequence, uncorrected photoluminescence overestimates the abundance of armchairlike tubes. We suggest experiments to verify our model, among them infrared Raman spectroscopy.

We thank A.C. Ferrari for discussions. S.R. was supported by the Oppenheimer Trust and Newnham College. This work was supported by the DFG (Th662/8-2) and the EPSRC (GR/S97613).

- [1] S. Reich, C. Thomsen, and J. Maultzsch, *Carbon Nanotubes: Basic Concepts and Physical Properties* (Wiley-VCH, Berlin, 2004).
- [2] S.M. Bachilo, M.S. Strano, C. Kittrell, R.H. Hauge, R.E. Smalley, and R.B. Weisman, *Science* **298**, 2361 (2002).
- [3] S. Lebedkin, F. Hennrich, T. Skipa, and M.M. Kappes, *J. Phys. Chem. B* **107**, 1949 (2003).
- [4] Y. Miyauchi, S. Chiashi, Y. Murakami, Y. Hayashida, and S. Maruyama, *Chem. Phys. Lett.* **387**, 198 (2004).
- [5] S. Reich and C. Thomsen, *Phys. Rev. B* **62**, 4273 (2000).
- [6] PL here refers to the combination of luminescence and luminescence excitation spectroscopy as normally done for nanotubes. ‘‘PL intensity’’ means the maximum intensity.
- [7] C.L. Kane and E.J. Mele, *Phys. Rev. Lett.* **90**, 207401 (2003).
- [8] G. Moos, C. Gahl, R. Fasel, M. Wolf, and T. Hertel, *Phys. Rev. Lett.* **87**, 267402 (2001).
- [9] R. Saito, G. Dresselhaus, and M.S. Dresselhaus, *Phys. Rev. B* **61**, 2981 (2000).
- [10] S. Reich, C. Thomsen, and P. Ordejón, *Phys. Rev. B* **65**, 155411 (2002).
- [11] V.N. Popov and L. Henrard, *Phys. Rev. B* **70**, 115407 (2004).
- [12] I. Milošević, T. Vuković, S. Dmitrović, and M. Damnjanović, *Phys. Rev. B* **67**, 165418 (2003).
- [13] A. Grüneis, R. Saito, G.G. Samsonidze, T. Kimura, M.A. Pimenta, A. Jorio, A.G.S. Filho, G. Dresselhaus, and M.S. Dresselhaus, *Phys. Rev. B* **67**, 165402 (2003).
- [14] J. Jiang, R. Saito, A. Grüneis, S.G. Chou, G.G. Samsonidze, A. Jorio, G. Dresselhaus, and M.S. Dresselhaus, *Phys. Rev. B* **71**, 045417 (2005).
- [15] C.L. Kane and E.J. Mele, *Phys. Rev. Lett.* **93**, 197402 (2004).
- [16] J.-S. Lauret, C. Voisin, G. Cassabois, C. Delalande, P. Roussignol, O. Jost, and L. Capes, *Phys. Rev. Lett.* **90**, 057404 (2003).
- [17] One might argue that the process in Fig. 1(c) creates two excitons and thus stronger PL. However,  $eh_{22} \rightarrow 2eh_{22}$  creates either two optically active or two dark excitons. We assume equal probability for both processes.
- [18] See EPAPS Document No. E-PRLTAO-95-044534 for the PL map without exciton resonances and a table of the exciton energies. This document can be reached via a direct link in the online article’s HTML reference section or via the EPAPS homepage (<http://www.aip.org/pubservs/epaps.html>).
- [19] S. Reich, J. Maultzsch, C. Thomsen, and P. Ordejón, *Phys. Rev. B* **66**, 035412 (2002).
- [20] V. Perebeinos, J. Tersoff, and P. Avouris, *Phys. Rev. Lett.* **92**, 257402 (2004).
- [21] H. Telg, J. Maultzsch, S. Reich, F. Hennrich, and C. Thomsen, *Phys. Rev. Lett.* **93**, 177401 (2004).
- [22] V.N. Popov, L. Henrard, and P. Lambin, *Nano Lett.* **4**, 1795 (2004).